Journal of Orthopaedic Surgery and Research

RESEARCH ARTICLE

Open Access

Local Application of Tanshinone IIA protects mesenchymal stem cells from apoptosis and promotes fracture healing in ovariectomized mice

Shao Cheng[1,2,3,4†], Xiaohui Hu[1,2,3†], Kanghui Sun[1,2,3†], Ziyu Huang[1,2,3], Yongjian Zhao[1,2,3], Yueli Sun[1,2,3], Bo Zeng[1,2,3], Jing Wang[3], Dongfeng Zhao[1,2,3], Sheng Lu[1,2,3], Qi Shi[1,2,3], Yongjun Wang[1,2,3], Weian Zhang[5*], Xinhua Liu[6*] and Bing Shu[1,2,3*]

Abstract

Background Elderly patients suffering from osteoporotic fractures are more susceptible to delayed union or nonunion, and their bodies then are in a state of low-grade chronic inflammation with decreased antioxidant capacity. Tanshinone IIA is widely used in treating cardiovascular and cerebrovascular diseases in China and has anti-inflammatory and antioxidant effects. We aimed to observe the antioxidant effects of Tanshinone IIA on mesenchymal stem cells (MSCs), which play important roles in bone repair, and the effects of local application of Tanshinone IIA using an injectable biodegradable hydrogel on osteoporotic fracture healing.

Methods MSCs were pretreated with or without different concentrations of Tanshinone IIA followed by H_2O_2 treatment. Ovariectomized (OVX) C57BL/6 mice received a mid-shaft transverse osteotomy fracture on the left tibia, and Tanshinone IIA was applied to the fracture site using an injectable hydrogel.

Results Tanshinone IIA pretreatment promoted the expression of nuclear factor erythroid 2-related factor 2 and antioxidant enzymes, and inhibited H_2O_2-induced reactive oxygen species accumulation in MSCs. Furthermore, Tanshinone IIA reversed H_2O_2-induced apoptosis and decrease in osteogenic differentiation in MSCs. After 4 weeks of treatment with Tanshinone IIA in OVX mice, the bone mineral density of the callus was significantly increased and the biomechanical properties of the healed tibias were improved. Cell apoptosis was decreased and Nrf2 expression was increased in the early stage of callus formation.

†Shao Cheng, Xiaohui Hu and Kanghui Sun contributed equally to this work.

*Correspondence:
Weian Zhang
wazhang@ecust.edu.cn
Xinhua Liu
healwa@163.com
Bing Shu
siren17721101@163.com

Full list of author information is available at the end of the article

Conclusions Taken together, these results indicate that Tanshinone IIA can activate antioxidant enzymes to protect MSCs from H_2O_2-induced cell apoptosis and osteogenic differentiation inhibition. Local application of Tanshinone IIA accelerates fracture healing in ovariectomized mice.

Keywords Tanshinone IIA, Osteoporotic fracture, Injectable hydrogel, Mesenchymal stem cell, Oxidative stress, Cell apoptosis, Nuclear factor erythroid 2-related factor 2

Background

Patients suffering from osteoporotic fractures, especially elderly individuals, are more susceptible to delayed union or nonunion, resulting in weakened biomechanical properties. Osteoporotic fractures represent the most serious complication of osteoporosis and are associated with higher disability and mortality rates than general fractures [1]. It is widely thought that by 2050, half of the global osteoporotic hip fractures will occur in Asia, imposing an enormous economic burden on medical and health expenditures [2].

During the early stages of fracture healing, the local environment, characterized by ischemia, hypoxia, and inflammation, results in the accumulation of reactive oxygen species (ROS), leading to increased oxidative stress levels. Generally, the antioxidant system clears these ROS to protect cells from oxidative damage [3–5]; however, in patients with osteoporosis, due to ageing, estrogen levels decline, and other factors, the body is in a state of low-grade chronic inflammation, and the antioxidant capacity of the body is decreased [6, 7]. Consequently, excessive and prolonged ROS activity at the fracture site can lead to cell cycle arrest and decreased osteogenic differentiation [8, 9], which are critical for bone regeneration during fracture healing.

Tanshinone IIA (CAS No. 568-72-9) is widely used for treating cardiovascular and cerebrovascular diseases in China. Tanshinone IIA has been confirmed to have anti-inflammatory, antioxidant, and other pharmacological effects [10–12]. Further studies with nerve cells, acinar cells, lung tissue, and myocardium revealed the involvement of the Kelch-like ech-associated protein-1 (Keap1)-nuclear factor erythroid 2-related factor 2 (Nrf2) pathway in the protective effects of Tanshinone IIA against ROS [13–15]. In addition, Tanshinone IIA can increase the recruitment of bone marrow mesenchymal stem cells (MSCs) and promote the osteogenic differentiation of MC3T3-E1 cells [16, 17]. Based on these findings, we hypothesized that Tanshinone IIA might be a potential candidate for treating osteoporotic fractures. Most of the previous studies on bone repair have focused on defects in flat bones or cortical bones, while there have been few studies on the treatment of long bone osteoporotic fractures, which have greater potential for clinical application.

In this study, we applied Tanshinone IIA to the fracture site in ovariectomized (OVX) mice using an injectable hydrogel and observed the effects of the local application of Tanshinone IIA on osteoporotic fracture healing. We also performed in vitro experiments to confirm the antioxidant effects of Tanshinone IIA on bone marrow MSCs.

Methods

Cell survival rate assessment

Tanshinone IIA (CAS No. 568-72-9) was purchased from Yuanye Biotechnology Co., Ltd (Shanghai, China). The purity of Tanshinone IIA was confirmed to be more than 98% by high-performance liquid chromatography. Primary bone marrow MSCs were plated in a 96-well plate at a density of 5×10^3 cells/well for 24 h and further treated with 0, 10^{-9}, 10^{-8}, 10^{-7}, 10^{-6} or 2×10^{-6}M Tanshinone IIA/dimethyl sulfoxide (DMSO) solutions for another 24 h. For H_2O_2 treatment, cells were plated in a 96-well plate at a density of 2×10^3 cells/well for 24 h and were pretreated with 2×10^{-6}M Tanshinone IIA or DMSO for another 24 h. Then, the medium was discarded, and the cells were incubated with 0, 50, 100, 200, 400, 500, 600, 800, or 1000μM H_2O_2 for 24 h. The cell survival rate was assessed with an enhanced cell counting kit-8 (C0041, Beyotime Biotechnology, Shanghai, China), and the absorbance at 450 nm was recorded by a microplate reader.

Osteogenic differentiation assay

Bone marrow cells from long bones of 4-week-old C57BL/6 mice were collected and plated in αMEM supplemented with 10% fetal bovine serum and 1% penicillin–streptomycin. After 7 days of culture, the suspended cells were removed, and the adherent cells were collected and plated in a 12-well plate at a density of 8×10^4 cells/well with osteogenic differentiation medium containing 50 mg/L vitamin C, 10nM dexamethasone, and 10mM β-glycerophosphate in complete αMEM. The cells were incubated with different concentrations of Tanshinone IIA with or without 500μM H_2O_2. The culture medium was refreshed every 3 days. After 10 days or 21 days culture, the cells were fixed with 10% buffered formalin for 15 min and stained with 1-step NBT/BCIP substrate solution (34,042, Thermo, Waltham, Massachusetts, USA) for 30 min or 0.1% Alizarin red (A5533, Sigma, St. Louis, Missouri, USA) aqueous solution for 30 min.

Real-time reverse transcriptase polymerase chain reaction (RT–PCR) assay

Primary bone marrow MSCs were plated in a 6-well plate at a density of 2×10^5 cells/well with osteogenic differentiation medium. Cells were treated with either 500μM H_2O_2 or 500μM H_2O_2 and different concentrations of Tanshinone IIA for 72 h. Total RNA of the cells was extracted using an RNA Extraction Kit (B0004D, HifunBio, Shanghai, China) and reverse transcribed to cDNA using an RT reagent kit (RR407, Takara Bio, Japan). PCR was performed using a TB Green Premix Ex Taq II kit (RR820, Takara Bio, Japan). The primers used for specific mRNAs are listed in Table 1.

Western blotting assay

$C_3H_{10}T_{1/2}$ cells provided by the National Collection of Authenticated Cultures, Chinese Academy of Sciences were plated in a 6-well plate at a density of 8×10^4 cells/well for 24 h and were pretreated with 0, 10^{-8}, 10^{-7}, or 10^{-6}M Tanshinone IIA for 24 h. After incubation in 500μM H_2O_2 for another 24 h, the cells were collected, and total proteins were extracted on ice using radioimmunoprecipitation assay lysis buffer (P0013B, Beyotime Biotechnology, Shanghai, China). The protein concentration was detected using an enhanced bicinchoninic acid assay kit (P0010, Beyotime Biotechnology, Shanghai, China). Western blot analysis was conducted as previously described [18]. The following antibodies were used: anti-cleaved caspase 3 (ab214430), anti-pro caspase 3 (ab32499), anti-superoxide dismutase 1 (SOD 1, ab13498), anti-heme oxygenase-1 (HO-1, ab68477), anti-catalase (CAT, ab16731) from Abcam (Cambridge, UK) and anti-Nrf2 (12721), anti-β-actin (8457), anti-Keap1 (8047), anti-Bcl2 (3498) and anti-Bax (5023) from Cell Signaling Technology (Danvers, Massachusetts, USA). A chemiluminescent horseradish peroxidase substrate kit (WBKLS0500, Millipore, Billerica, Massachusetts, USA) was used for the electrochemiluminescence detection assay.

Detection of antioxidant enzymes

$C_3H_{10}T_{1/2}$ cells were plated in a 12-well plate or 6-well plate for 24 h. After pretreatment with different concentrations of Tanshinone IIA or DMSO for 24 h, the cells were incubated in fresh medium supplemented with 500μM H_2O_2 for another 24 h. For ROS detection, the cells were incubated in αMEM containing a 10mM 2,7-dichlorodihydrofluorescein diacetate (H_2DCFDA) fluorescence probe (287810, Sigma, St. Louis, Missouri, USA) for 30 min, and the fluorescence intensity was measured by flow cytometry (Accuri C6, BD Biosciences, Franklin Lakes, New Jersey, USA). SOD and CAT activity in cells was detected using relative activity test kits (SOD, S0101S; CAT, S0051; Beyotime Biotechnology, Shanghai, China).

Table 1 PCR primers for specific genes

Genes	primer sequences	
β-actin	Forward	5′- TATCGCTGCGCTGGTCG – 3′
	Reverse	5′- CCCACGATGGAGGGGAATAC – 3′
Runx2	Forward	5′- GTGGCAGTGTCATCATCTGAAAT – 3′
	Reverse	5′-TCGCCTCAGTGATTTAGGGCGCA-3′
osterix	Forward	5′- TGCTATACTCTGGGGGCTCTC – 3′
	Reverse	5′- AGGAGGTCGGAGCATAGGAA – 3′

Immunofluorescence staining

$C_3H_{10}T_{1/2}$ cells were plated in a 48-well plate and cultured with 0, 10^{-8}, 10^{-7}, or 10^{-6}M Tanshinone IIA for 24 h, followed by culture in fresh medium supplemented with 500μM H_2O_2 for another 24 h. After fixation with 4% formaldehyde solution at 37℃ for 15 min, the cells were incubated with an Nrf2 antibody (12721, Cell Signaling Technology, Danvers, Massachusetts, USA, 1:500) overnight at 4℃. Cells were further incubated in CoraLite594-conjugated goat anti-rabbit IgG (SA00013-4; Proteintech, Wuhan, Hubei, China; 1:200) for 1 h at 37℃ in the dark. Antifade mounting medium with 4,6-diamidino-2-phenylindole (DAPI) was used for nuclear fluorescence staining (H-1200, Vector Laboratories, San Francisco, California, USA).

Animals

The study was conducted according to the guidelines of the Declaration of Helsinki, and approved by the Institutional Animal Care and Use Committee of Longhua Hospital, Shanghai University of Traditional Chinese Medicine (2019-N051). Three-month-old female C57BL/6 mice (21–23 g body weight) ordered from Lingchang Biotech (Shanghai, China) were housed at 22˚C with a 12 h light/dark cycle, with 4 or fewer mice in each cage, and were provided *ad libitum* access to food and water in the specific pathogen-free animal experiment center of Longhua Hospital.

Grouping and model establishment

Following a 1-week acclimatization phase, the mice were randomly assigned to the sham, model, gel, and Tanshinone IIA groups using a random number table. Mice in the model, gel, and Tanshinone IIA groups underwent bilateral ovariectomy, and the rest underwent sham operations. Three months after the surgery, all mice received a mid-shaft transverse osteotomy fracture on the left tibias, and the tibias were fixed with 0.5-mm-diameter intramedullary metallic pins. Anesthesia was induced in mice by isoflurane inhalation through an inhalation anesthesia machine before surgery.

Hydrogel preparation and intervention

The injectable hydrogel was prepared as previously described [19]. A filtered 40 mg/ml dextran/phosphate buffered saline (PBS) solution containing 4μM Tanshinone IIA/DMSO or an equal volume of DMSO and 20 mg/ml filtered chitosan/PBS solution was prepared. When setting up the fracture model, the dextran/PBS solution and chitosan/PBS solution were mixed at a 1:1 ratio, and 20 μl of semisolidified hydrogel was injected into the bilateral bone marrow cavities of the fracture ends before fixing the tibias with pins. Mice in the Tanshinone IIA group were injected with a hydrogel containing 2μM Tanshinone IIA, and mice in the gel group received a hydrogel containing DMSO.

Sample harvest

Mice were sacrificed at the corresponding time points. Mice were anesthetized with isoflurane in an induction chamber, followed by intraperitoneal injection of pentobarbital sodium (5.4 g/kg body weight). The left tibias (6 from each group per time point) were fixed in 10% buffered formalin and subjected to micro-computed tomography (micro-CT) scanning. After decalcification, dehydration, and embedding, 4 μm thick serial sections of the tibias were cut for histomorphometric evaluation. Another set of 5 tibias from each group was harvested 28 days postfracture and stored at -80°C for biomechanical testing.

Biomechanical test

The tibias were equilibrated with saline at room temperature before assessment. A three-point mechanical bending test was performed on the left tibias to assess the maximum force and yield displacement with a mechanical testing instrument (ElectroForce 3200 Series III, TA Instrument, New Castle, Delaware, USA).

Threedimensional (3D) reconstruction analyses

The fractured tibias were subjected to X-ray imaging and micro-CT scanning (vivaCT 40, Scanco Medical AG, Brüttisellen, Switzerland) successively at a voltage of 55 kV and a current of 72μA. The integration time was 300ms, and the slice increment was 10 mm. The bone volume (BV, mm^3), total volume (TV, mm^3), bone mineral density (BMD), trabecular bone number (Tb.N), trabecular bone thickness (Tb.Th), and trabecular bone separation (Tb.Sp) of the callus were measured.

Histological evaluation

For morphometric analysis, midsagittal sections of the tibias were dewaxed and stained with Alcian blue/hematoxylin solution and orange G solution. After dehydration, clearing, and mounting, images of the sections were captured by a virtual slide system (VS120-S6-W, Olympus, Japan).

TdT-mediated dUTP Nick End Labelling (TUNEL)

$C_3H_{10}T_{1/2}$ cells were plated in a 48-well plate at a density of 1×10^4 cells/well for 24 h and were pretreated with 0, 10^{-8}, 10^{-7}, or 10^{-6}M Tanshinone IIA for 24 h. After incubation in 500μM H_2O_2 for another 24 h, cells were fixed with 4% formaldehyde at 37℃ for 30 min. For the animal study, midsagittal sections of the callus were dewaxed and rehydrated. TUNEL staining was performed using a staining kit (C1088, Beyotime Biotechnology, Shanghai, China), and cell apoptosis was observed using a fluorescence microscope and were analyzed with an image Pro Plus 6.0 software (Media Cybernetics, PA, USA).

Immunohistochemical staining

After dewaxing and rehydration, sections were treated with 3% H_2O_2 solution for 15 min at 37 °C, followed by the antigen repair with sodium citrate solution for 15 min at 95 °C. The sections were incubated in primary Nrf2 antibody (16396-1-AP, Wuhan Sanying, Wuhan, China, 1:100) overnight at 4 °C. The sections were then incubated in horseradish peroxidase labeled goat anti rabbit IgG (A0208, Beyotime Biotechnology, Shanghai, China) for 40 min. After staining with diaminobenzidine and counterstaining with hematoxylin, the images were captured by by a virtual slide system (VS120-S6-W, Olympus, Japan), and were analyzed with an image Pro Plus 6.0 software (Media Cybernetics, PA, USA).

Statistical analyses

All of the data are presented as the means±standard deviations. Statistical analyses and graph generation were performed using GraphPad Prism 8 (GraphPad Software, San Diego, California, USA). The normality of the data was assessed by the Shapiro–Wilk test, and the homogeneity of variance was tested. For data with homogeneity and normality, statistical significance among multiple groups was assessed by one-way analysis of variance (ANOVA). Otherwise, the Kruskal–Wallis H test was used. A P value<0.05 was considered to indicate statistical significance.

Results

Tanshinone IIA mitigated H_2O_2-induced apoptosis in MSCs

To assess the safety of Tanshinone IIA, primary bone marrow MSCs were treated with different concentrations of Tanshinone IIA solutions. Tanshinone IIA solution at a concentration of 2×10^{-6}M or less showed no cytotoxicity compared with the negative control group (Fig. 1a). When bone marrow MSCs were treated with Tanshinone IIA, *Runx2* (10^{-6}M and 10^{-7}M groups) and *osterix* (10^{-6}M groups) expression levels were slightly increased (Fig. 1b).

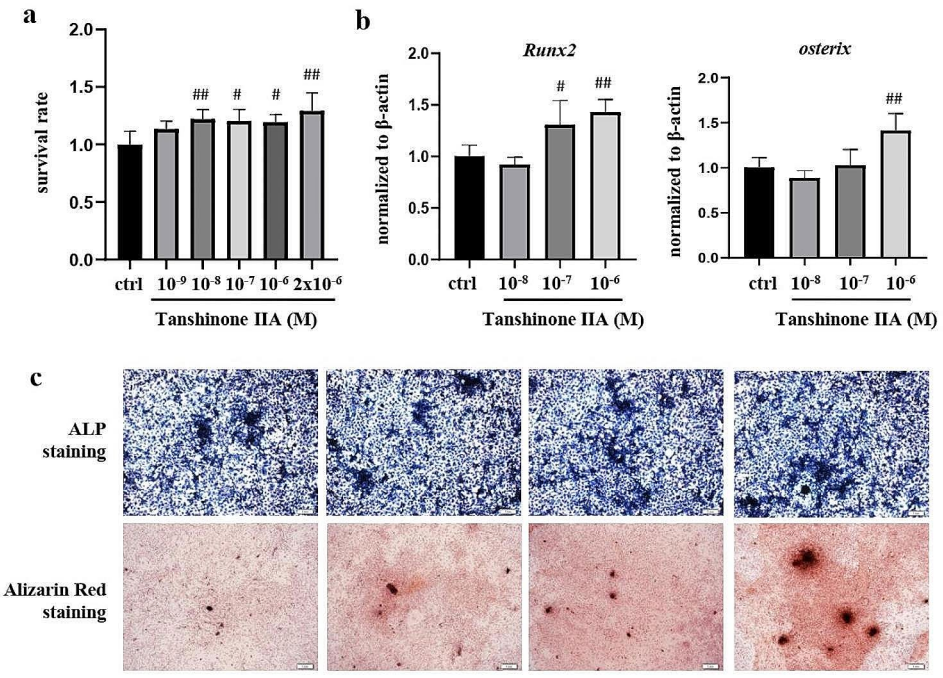

Fig. 1 Effects of Tanshinone IIA on the osteogenic differentiation of primary bone marrow MSCs. Primary bone marrow MSCs were treated with different concentrations of Tanshinone IIA for 24 h. **(a)** Survival rates of primary bone marrow MSCs. **(b)** The gene expression levels of Runx2 and osterix in primary bone marrow MSCs. **(c)** Images of ALP staining and Alizarin Red staining of primary bone marrow MSCs. MSC, mesenchymal stem cell. ALP, alkaline phosphatase. All experiments were repeated at least 3 times. Compared with the ctrl group, #, $p < 0.05$; ##, $p < 0.01$

Additionally, the osteogenic differentiation ability and mineralization ability of the cells were slightly increased in the group treated with the high concentration of Tanshinone IIA (Fig. 1c).

After treatment with different concentrations of H_2O_2 for 24 h, the percentage of surviving cells gradually decreased with increasing H_2O_2 concentration, with the most significant decrease observed in the range of 300μM–600μM H_2O_2. However, pretreatment with 2×10^{-6}M Tanshinone IIA for 24 h significantly reversed the decrease in survival rate in 500μM H_2O_2-treated cells, suggesting that Tanshinone IIA has a protective effect on cell survival within a certain range (Fig. 2a). TUNEL staining revealed that 500μM H_2O_2 induced significant cell apoptosis, while pretreatment with a high dose of Tanshinone IIA (10^{-7}M and 10^{-6}M) for 24 h significantly decreased H_2O_2-induced apoptosis in $C_3H_{10}T_{1/2}$ cells (Fig. 2b and c). Changes in the expression levels of cell apoptosis-related proteins were further investigated. Pretreatment with a high dose of Tanshinone IIA inhibited the H_2O_2-induced increase in cleaved caspase 3/pro caspase 3 and Bax/Bcl2 in $C_3H_{10}T_{1/2}$ cells (Fig. 2d and e).

Tanshinone IIA reversed the H_2O_2-induced decrease in osteogenic differentiation in primary bone marrow MSCs

To evaluate the effects of Tanshinone IIA under oxidative stress, primary bone marrow MSCs were further treated sequentially with different concentrations of Tanshinone IIA for 24 h and 500μM H_2O_2. H_2O_2 treatment dramatically impaired the ability of primary bone marrow MSCs to undergo osteogenic differentiation and mineralization, and pretreatment with Tanshinone IIA reversed the decrease induced by H_2O_2 in a dose-dependent manner (Fig. 3a). In addition, the H_2O_2-induced decreases in the gene expression levels of Runx2 and osterix were reversed by Tanshinone IIA pretreatment (Fig. 3b).

Tanshinone IIA promoted Nrf2 and antioxidant enzyme expression in MSCs

To observe the antioxidant effects of Tanshinone IIA, $C_3H_{10}T_{1/2}$ cells were pretreated with different concentrations of Tanshinone IIA for 24 h, followed by H_2O_2 stimulation for another 24 h. Tanshinone IIA significantly inhibited H_2O_2-induced ROS accumulation in $C_3H_{10}T_{1/2}$ cells in a dose-dependent manner (Fig. 4a). The activity of antioxidant enzymes in $C_3H_{10}T_{1/2}$ cells, including SOD and CAT, was increased by treatment with a high concentration (10^{-6}M) of Tanshinone IIA compared with that in the H_2O_2 group (Fig. 4a). Western Blotting assays and quantitative analyses also confirmed increased SOD 1, HO-1, and CAT expression levels in $C_3H_{10}T_{1/2}$ cells (Fig. 4b-c). The Keap1/Nrf2 signalling pathway is the main defence mechanism against oxidative stress mediated by the regulation of antioxidant enzyme synthesis. Western blotting assays demonstrated that treatment with a high concentration of Tanshinone IIA increased

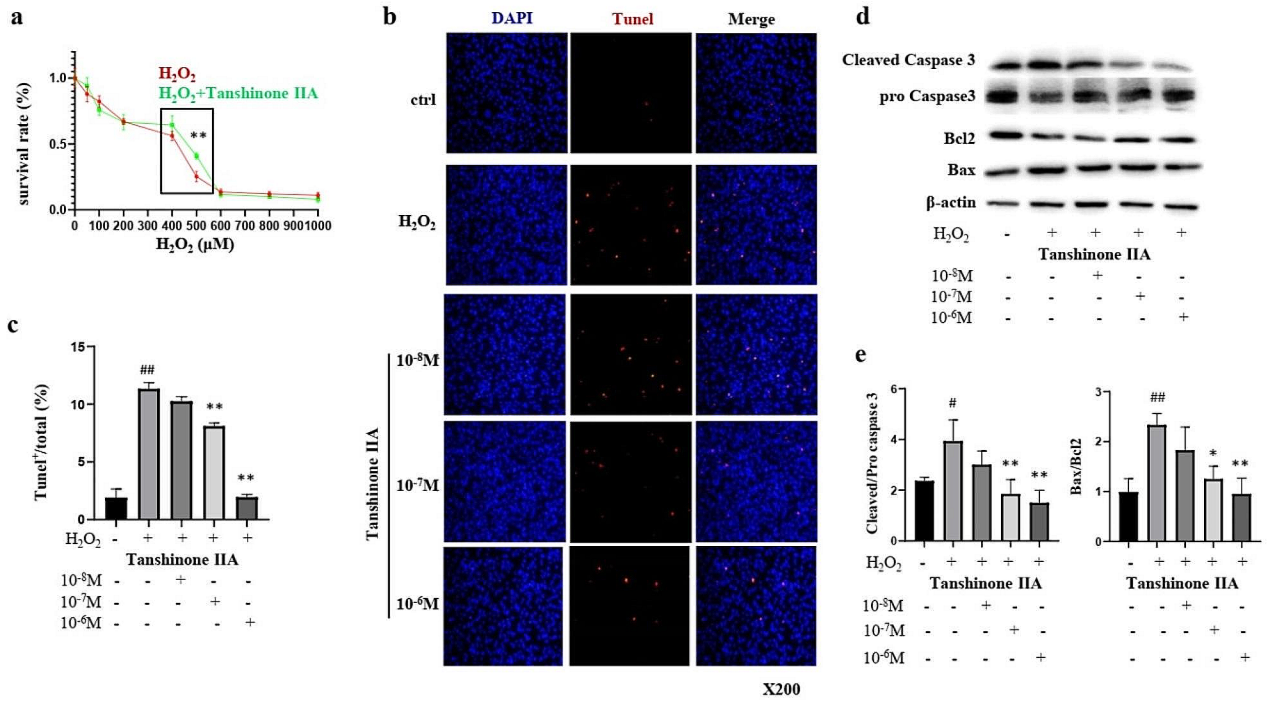

Fig. 2 Tanshinone IIA inhibited H_2O_2-induced apoptosis in MSCs. **a)** Survival rates of $C_3H_{10}T_{1/2}$ cells sequentially pretreated with 2×10^{-6}M Tanshinone IIA for 24 h and different concentrations of H_2O_2 for 24 h. **b**, **c**) $C_3H_{10}T_{1/2}$ cells were pretreated with different concentrations of Tanshinone IIA for 24 h and then treated with 500μM H_2O_2 for another 24 h. TUNEL staining for cell apoptosis and quantification of the proportions of $TUNEL^+$ cells among the total cells are shown. **d**, **e**) $C_3H_{10}T_{1/2}$ cells were pretreated with different concentrations of Tanshinone IIA for 24 h and then treated with 500 μM H_2O_2 for another 24 h. Western blotting assays and quantification for cell apoptosis-related proteins are shown. MSC, mesenchymal stem cell. TUNEL, TdT-mediated dUTP nick end labelling method. All experiments were repeated at least 3 times. H_2O_2 group vs. negative control group, #, $p<0.05$; ##, $p<0.01$. Tanshinone IIA groups vs. H_2O_2 group, *, $p<0.05$; **, $p<0.01$

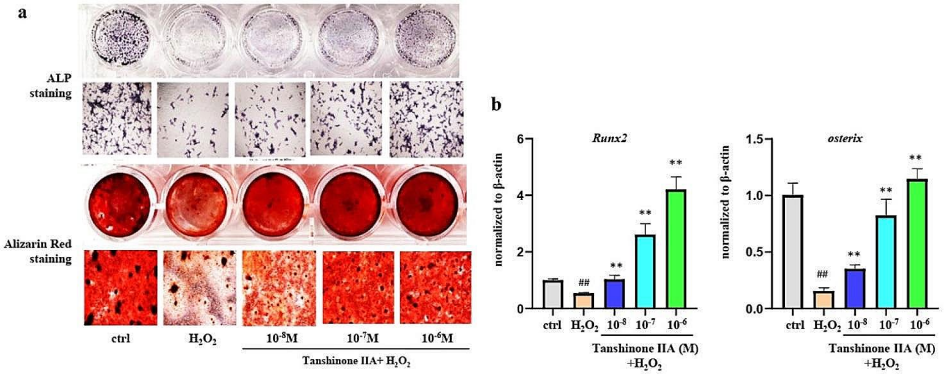

Fig. 3 Tanshinone IIA reversed the H_2O_2-induced decrease in osteogenic differentiation in primary bone marrow MSCs. Primary bone marrow MSCs pretreated with Tanshinone IIA for 24 h were further treated with 500μM H_2O_2. **(a)** Images of ALP staining and Alizarin Red staining showing the osteogenic differentiation and mineralization of primary bone marrow MSCs. **(b)** The gene expression levels of Runx2 and osterix in primary bone marrow MSCs. MSC, mesenchymal stem cell. ALP, alkaline phosphatase. All experiments were repeated at least 3 times. H_2O_2 group vs. ctrl group, ##, $p<0.01$. Tanshinone IIA groups vs. H_2O_2 group, **, $p<0.01$

Nrf2 expression in H_2O_2-treated $C_3H_{10}T_{1/2}$ cells but had no effect on Keap1 expression (Fig. 4d and e). Immunofluorescence staining for Nrf2 also revealed increased Nrf2 expression in $C_3H_{10}T_{1/2}$ cells treated with a high concentration of Tanshinone IIA (Fig. 4f and g).

Local application of Tanshinone IIA promoted fracture healing in OVX mice

As shown by the X-ray and 3D reconstruction images, 2 weeks after fracture, significant callus formation was observed in the tibias of mice from the sham group and Tanshinone IIA group, while mice in the model group

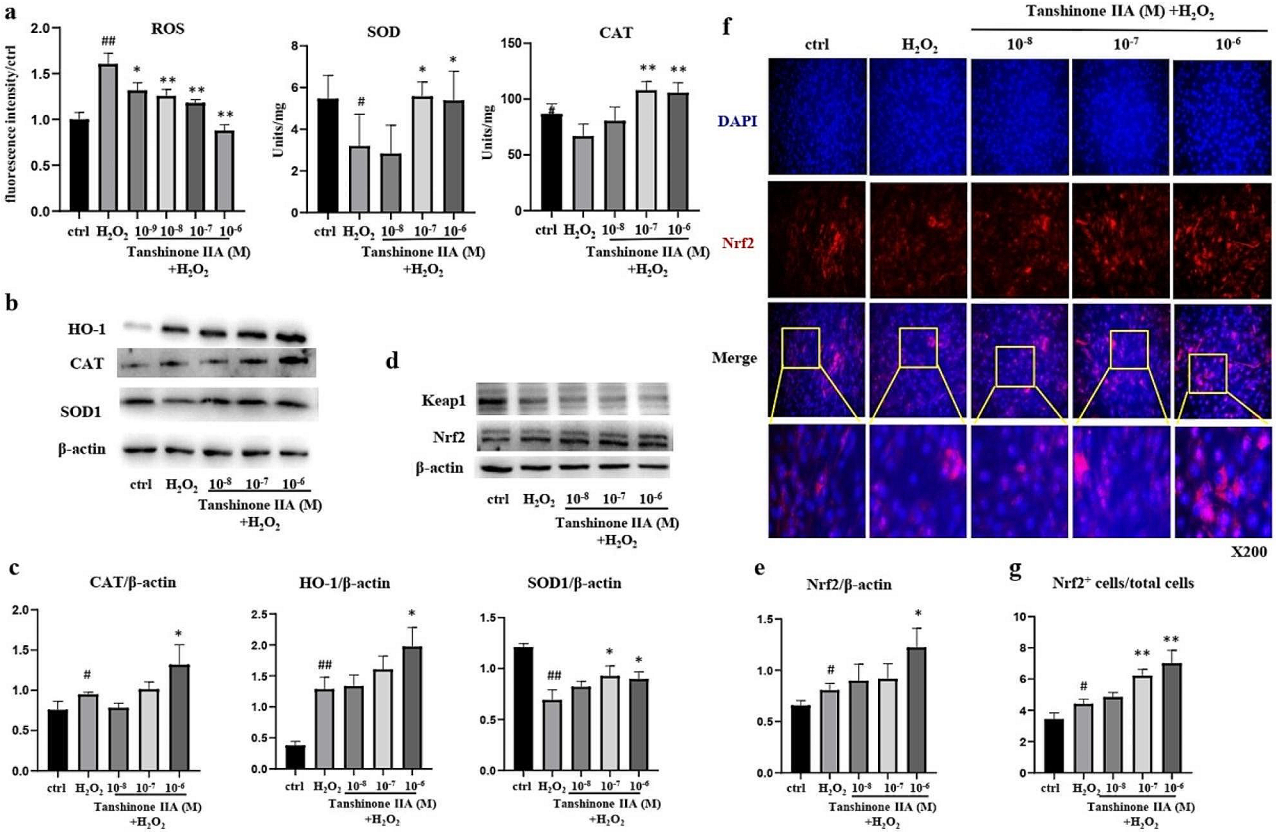

Fig. 4 Tanshinone IIA increased Nrf2 and antioxidant enzyme expression in $C_3H_{10}T_{1/2}$ cells. $C_3H_{10}T_{1/2}$ cells were pretreated with different concentrations of Tanshinone IIA for 24 h, followed by stimulation with 500μM H_2O_2 for another 24 h. **a)** ROS levels and the enzyme activities of SOD and CAT in $C_3H_{10}T_{1/2}$ cells. **b**, **c**) Western blotting assays and quantification of SOD, HO-1, and CAT in $C_3H_{10}T_{1/2}$ cells. **d**, **e**) Western blotting assays and quantification of Keap1 and Nrf2 expression in $C_3H_{10}T_{1/2}$ cells. **f**, **g**) Immunofluorescence staining for Nrf2, and quantification of the proportions of $Nrf2^+$ cells in total $C_3H_{10}T_{1/2}$ cells. SOD, superoxide dismutase; HO-1, heme oxygenase-1; CAT, catalase; Nrf2, nuclear factor erythroid 2-related factor 2. All experiments were repeated at least 3 times. H_2O_2 group vs. ctrl group, #, $p < 0.05$; ##, $p < 0.01$. Tanshinone IIA groups vs. H_2O_2 group, *, $p < 0.05$; **, $p < 0.01$

and gel group exhibited less callus formation. Four weeks after fracture, small calluses with smooth and continuous cortical bone were found in sham mice and Tanshinone IIA-treated mice, while the model and gel groups exhibited large calluses, suggesting accelerated bone fracture healing in OVX mice after Tanshinone IIA treatment (Fig. 5a and b). Compared with those in the sham group, the BMD, BV/TV, Tb.N, and Tb.Th of the callus in the model group were significantly lower, while the Tb. Sp was higher at 4 weeks after the fracture. After 4 weeks of treatment with Tanshinone IIA, the BMD and BV/TV significantly increased compared with those of the model group and gel group (Fig. 5c). Histological staining also confirmed the improved microstructure of the callus with a smaller callus and smoother cortical bone at 28 days postfracture after Tanshinone IIA treatment (Fig. 6a and b). Biomechanical tests revealed greater maximum force and yield displacement in the Tanshinone IIA-treated mice than those in the model mice 4 weeks after treatment (Fig. 6c and d). To confirm the antiapoptotic effect of Tanshinone IIA in vivo, TUNEL staining was performed on 7-day callus from each group. The dramatical increase in cell apoptosis in the callus of the model group was partially alleviated in Tanshinone IIA group (Fig. 6e and f). IHC staining also confirmed the evalutated Nrf2 expression in the callus of the Tanshinone IIA group compared with that of the model group in the early stage of fracture healing (Fig. 6g and h).

Discussion

Osteoporosis is characterized by an increased level of reactive oxygen species in the bone microenvironment [20]. Ageing and decrease in ovarian function with menopause, the main causes of osteoporosis, have been associated with spontaneous increases in proinflammatory cytokines, resulting in chronic low-grade systemic inflammation [21, 22]. Ageing, menopause, and proinflammatory cytokines have been shown to regulate ROS levels in cells and tissues, leading to oxidative stress [23, 24]. On the other hand, oxidative stress may enhance the expression of genes involved in inflammation and lead to ageing and estrogen deficiency [25, 26]. These factors

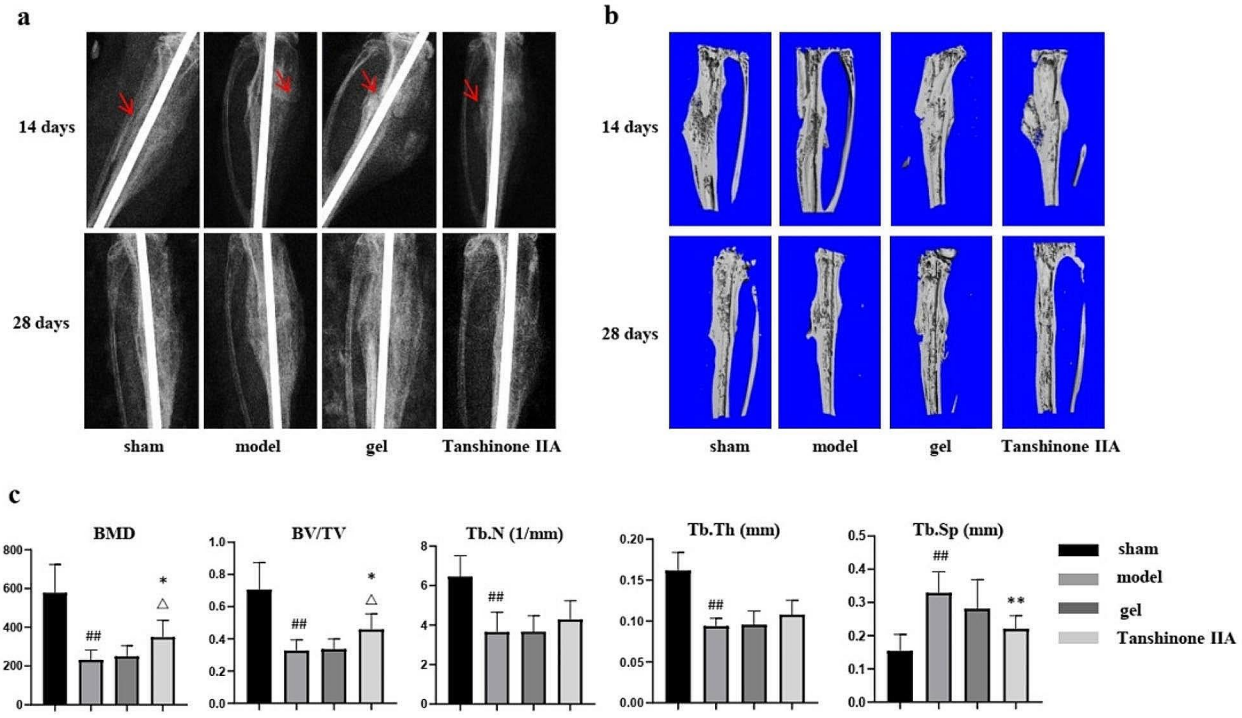

Fig. 5 Tanshinone IIA improved the bone mineral density and microstructure of the callus in OVX mice. **(a)** X-ray images of the fracture sites in mice in different groups 14 days and 28 days postfracture. Arrows, fracture lines. **(b)** Sectional views of the callus reconstructed by micro-CT analyses 14 days and 28 days postfracture. **(c)** Quantitative analyses of bone mass and trabecular parameters of the callus in mice in different groups 28 days postfracture. $n = 6$. OVX, ovariectomized. Model group vs. sham group, ##, $p < 0.01$. Tanshinone IIA group vs. model group, *, $p < 0.05$; **, $p < 0.01$. Tanshinone IIA group vs. gel group, △, $p < 0.05$

act synergistically to promote pathophysiological risks throughout the body and contribute to the onset of disease [27–29].

MSCs are adult stem cells with the potential to differentiate into mesodermal lineages and play an important role in tissue homeostasis and regeneration. During fracture healing, MSCs recruited from bone marrow or other adjacent tissues to the injured site undergo proliferation and differentiation into osteoblasts and chondrocytes and dominate the process of bone formation through intramembrane ossification and endochondral ossification [30]. During the early stages after fracture, the microenvironment at the fracture site experiences mild ischemia, hypoxia, and local inflammation due to blood vessel and soft tissue damage, leading to ROS accumulation and increased oxidative stress levels [31, 32]. Generally, these ROS can be cleared by the body's antioxidant system, protecting surrounding cells, including MSCs, from oxidative damage [33]. Moreover, ROS at the physiological level may play important physiological roles in the process of fracture healing by targeting resident cells, including MSCs [34, 35]; however, during osteoporosis, when ROS levels exceed physiological levels, a high oxidative environment facilitates MSC senescence by inducing mitochondrial dysfunction, resulting in decreased proliferation, increased apoptosis, and decreased osteogenic differentiation [36–38], which may inhibit or delay the fracture healing process.Therefore, protecting MSCs from excessive oxidative impairment and promoting their differentiation ability during osteoporotic fracture healing are important.

Tanshinone IIA is a commonly used Chinese medicine that has significant effects on treating cardiovascular system diseases. Previous studies have revealed the beneficial effects of Tanshinone IIA in both healthy animals and animal models of bone loss [39–44]. However, there are few studies on the use of Tanshinone IIA for bone repair. In addition, most in vitro studies have focused on the function of Tanshinone IIA in inhibiting osteoclastogenesis [39–41], with little emphasis on its role in MSC osteogenic differentiation or osteoblast survival. Tanshinone IIA (1μM and 5μM) promoted the osteogenesis of mouse bone marrow MSCs at both the early and late stages; however, 20μM Tanshinone IIA inhibited osteogenesis [17]. In addition, it has been shown that Tanshinone IIA can reverse dexamethasone-induced cell apoptosis in MC3T3-E1 or H_2O_2-induced osteoblast apoptosis, which might be related to the inhibition of Nox4-mediated ROS production or the nuclear factor kappa-B signalling pathway [45, 46].

In this study, we used H_2O_2 to induce excessive oxidative stress in MSCs and confirmed that Tanshinone IIA

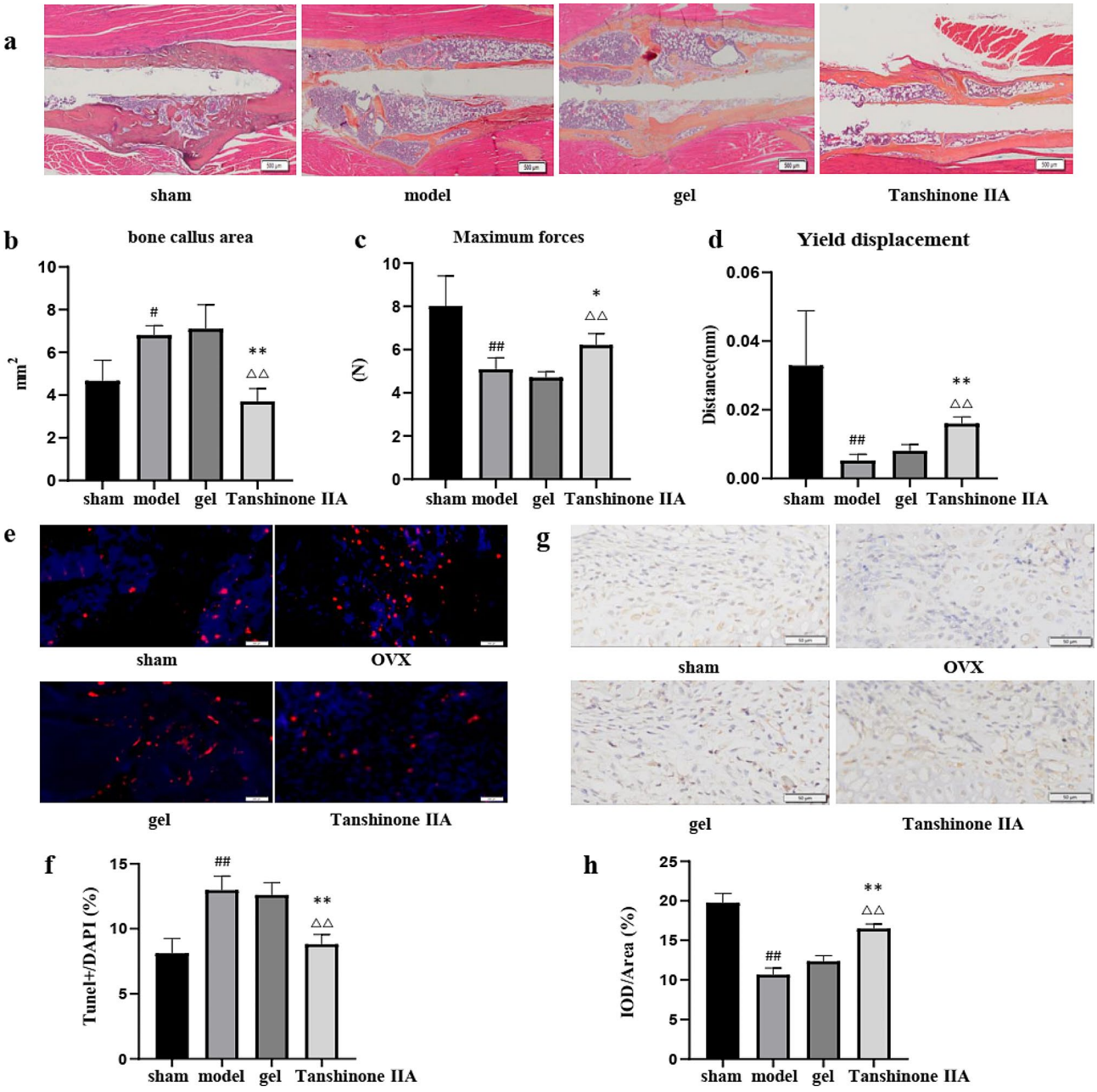

Fig. 6 Tanshinone IIA improved the histopathological structure and biomechanical properties of the callus in OVX mice. **a**, **b**) Alcian blue/hematoxylin/orange G staining of the callus and quantitative analyses of the callus area in mice in different groups 28 days postfracture. $n = 3$. Maximum forces **c**) and yield displacement **d**) of the tibias of mice in different groups 28 days postfracture. $n = 5$. **e**, **f**) TUNEL staining of the callus of different groups 7 days postfracture. $n = 3$. **g**, **h**) IHC for Nrf2 expression with the callus of different groups 7 days postfracture. $n = 3$. OVX, ovariectomized. Model group vs. sham group, #, $p < 0.05$; ##, $p < 0.01$. Tanshinone IIA group vs. model group, *, $p < 0.05$; **, $p < 0.01$. Tanshinone IIA group vs. gel group, △△, $p < 0.01$

at relatively low concentrations exerted protective effects by reversing H_2O_2-induced cell apoptosis and rescued H_2O_2-induced decreases in the osteogenic differentiation and mineralization of MSCs. Furthermore, we confirmed that Tanshinone IIA could increase antioxidant enzyme production and reduce ROS level in H_2O_2 treated MSCs, contributing to the antioxidative and antiapoptotic functions of Tanshinone IIA.

Keap1-Nrf2 signalling regulates the activation of various genes that protect cells from oxidative stress. Nrf2 activity is mainly regulated by Keap1 in response to oxidative stress. Under nonstress conditions, Nrf2 is sequestered in the cytoplasm by Keap1. However, under stress conditions, ROS interrupts Keap1-Nrf2 binding, which is followed by the nuclear translocation of Nrf2 and the transcription of target genes, including antioxidant

enzymes [47, 48]. In the present study, we further clarified that Tanshinone IIA increased Nrf2 expression in MSCs and enhanced the production of antioxidant enzymes, including HO-1, CAT, and SOD1; however, the protein level of Keap1 was not significantly changed, suggesting that the regulation of Nrf2 by Tanshinone IIA may be independent of Keap1, highlighting the complexity of the underlying mechanisms involved.

It is now understood that Tanshinone IIA has limited bioavailability when administered orally [49], suggesting poor absorption or significant metabolism. Hydrogels are a group of materials with three-dimensional cross-linked network structures that can mimic the natural extracellular matrix, facilitating cell growth and nutrient transport. Chitosan/dextran-based hydrogels have been proven to have appropriate biocompatibility, biodegradability and mechanical properties, as well as negligible cytotoxicity, minimal swelling and definite efficacy as drug delivery vehicles [50–54]. In addition, it would be of great simplicity and clinical importance to treat patients with undisplaced fractures or repositioned fractures with an injection to the site of injury [55]. Therefore, we employed an injectable biodegradable hydrogel as a delivery system for the local release of Tanshinone IIA at fracture sites. By utilizing this approach in a fracture model using OVX mice, we demonstrated that the local application of Tanshinone IIA promoted fracture healing and improved the biomechanical properties of the bones. Furthermore, this treatment approach could be applied to patients with osteoporotic fractures.

In conclusion, we provided compelling evidence that Tanshinone IIA could promote Nrf2 expression and activate antioxidant enzymes during H_2O_2-induced oxidative stress to protect MSCs from cell apoptosis and osteogenic differentiation inhibition. In vivo, local application of Tanshinone IIA accelerated fracture healing in OVX mice.

Although antioxidation appears to be one of the mechanisms through which Tanshinone IIA facilitates this process, it is highly conceivable that multiple other pathways are likely involved. These effects may include anti-inflammatory effects and the promotion of angiogenesis. Further investigations are required to fully elucidate the comprehensive mechanisms underlying the regulatory effects of Tanshinone IIA on fracture healing.

Abbreviations

MSC	Mesenchymal stem cells
OVX	Ovariectomized
ROS	Reactive oxygen species
Keap1	Kelch-like ech-associated protein-1
Nrf2	Nuclear factor erythroid 2-related factor 2
DMSO	Dimethyl sulfoxide
MEM	Minimum essential medium
RT-PCR	Reverse transcriptase polymerase chain reaction
SOD	Superoxide dismutase
HO-1	Heme oxygenase-1
CAT	Catalase
H_2DCFDA	2,7-dichlorodihydrofluorescein diacetate
DAPI	4,6-diamidino-2-phenylindole
PBS	Phosphate buffered saline
CT	Computed tomography
BV	Bone volume
TV	Total volume
BMD	Bone mineral density
Tb. N	Trabecular number
Tb. Th	Trabecular thickness
Tb. Sp	Trabecular separation
TUNEL	TdT-mediated dUTP nick end labeling
ANOVA	Analysis of variance
ALP	Alkaline phosphatase
Runx2	Runt-related transcription factor 2

Author contributions

SC, XH, KS collected and analyzed the data, and drafted the manuscript. ZH, YZ, YS, BZ and DZ collected the data. JW and SL analyzed the data. QS, YW and WZ participated in the design of the study. XL and WZ participated in the design and revision the manuscript. BS participated in the design, the data analyses, and drafting and revision of the manuscript. All authors have read and approved the final submitted manuscript.

Funding

This work was partially supported by the Key Science and Technology Project in Xinjiang Autonomous Region (2023A03007), the National Natural Science Foundations of China (81929004, 81973876, 82274555), the Natural Science Foundation of Henan Province (232300420269), Henan Province Project of Traditional Chinese Medicine Scientific Research (2022ZY2026) and the Key Research Program of Henan Colleges and Universities (24A360002).

Data availability

Dataset available on request from the authors.

Declarations

Competing interests

The authors declare no competing interests.

Author details

[1]Longhua Hospital, Shanghai University of Traditional Chinese Medicine, Shanghai 200032, China
[2]Spine Institute, Shanghai Academy of Traditional Chinese Medicine, Shanghai 200032, China
[3]Key Laboratory, Ministry of Education of China, Shanghai 200032, China
[4]School of Orthopedics, Henan University of Chinese Medicine, Zhengzhou 450002, China
[5]Shanghai Key Laboratory of Functional Materials Chemistry, East China University of Science and Technology, Shanghai 200237, China
[6]Shanghai University of Traditional Chinese Medicine, Shanghai 201203, China

Received: 8 April 2024 / Accepted: 10 May 2024
Published online: 23 May 2024

References

1. Bliuc D, Nguyen ND, Nguyen TV, Eisman JA, Center JR. Compound risk of high mortality following osteoporotic fracture and refracture in elderly women and men. J Bone Min Res. 2013;28:2317–24.
2. Si L, Winzenberg TM, Jiang Q, Chen M, Palmer AJ. Projection of osteoporosis-related fractures and costs in China: 2010–2050. Osteoporos Int. 2015;26:1929–37.
3. Wang Z, Ehnert S, Ihle C, Schyschka L, Pscherer S, Nussler NC, et al. Increased oxidative stress response in granulocytes from older patients with a hip fracture may account for slow regeneration. Oxid Med Cell Longev. 2014;2014:819847.

4. Ilyas A, Odatsu T, Shah A, Monte F, Kim HK, Kramer P, et al. Amorphous silica: a new antioxidant role for Rapid critical-sized bone defect Healing. Adv Healthc Mater. 2016;5:2199–213.
5. Kubo Y, Wruck CJ, Fragoulis A, Drescher W, Pape HC, Lichte P, et al. Role of Nrf2 in Fracture Healing: clinical aspects of oxidative stress. Calcif Tissue Int. 2019;105:341–52.
6. Manolagas SC. From estrogen-centric to aging and oxidative stress: a revised perspective of the pathogenesis of osteoporosis. Endocr Rev. 2010;31:266–300.
7. Zhang YB, Zhong ZM, Hou G, Jiang H, Chen JT. Involvement of oxidative stress in age-related bone loss. J Surg Res. 2011;169:e37–42.
8. Bigarella CL, Liang R, Ghaffari S. Stem cells and the impact of ROS signaling. Development. 2014;141:4206–18.
9. Atashi F, Modarressi A, Pepper MS. The role of reactive oxygen species in mesenchymal stem cell adipogenic and osteogenic differentiation: a review. Stem Cells Dev. 2015;24:1150–63.
10. Liu QY, Zhuang Y, Song XR, Niu Q, Sun QS, Li XN, et al. Tanshinone IIA prevents LPS-induced inflammatory responses in mice via inactivation of succinate dehydrogenase in macrophages. Acta Pharmacol Sin. 2021;42:987–97.
11. Wang X, Wang WM, Han H, Zhang Y, Liu JL, Yu JY, et al. Tanshinone IIA protected against lipopolysaccharide-induced brain injury through the protective effect of the blood-brain barrier and the suppression of oxidant stress and inflammatory response. Food Funct. 2022;13:8304–12.
12. Rao S, Lin Y, Lin R, Liu J, Wang H, Hu W, et al. Traditional Chinese medicine active ingredients-based selenium nanoparticles regulate antioxidant selenoproteins for spinal cord injury treatment. J Nanobiotechnol. 2022;20:278.
13. Zhu X, He L, Gao W, Zhao Z. Neuroprotective investigation of tanshinone in the cerebral infarction model in the Keap1-Nrf2/ARE pathway. Cell Cycle. 2022;1–13.
14. Chen W, Yuan C, Lu Y, Zhu Q, Ma X, Xiao W, et al. Tanshinone IIA protects against Acute Pancreatitis in mice by inhibiting oxidative stress via the Nrf2/ROS pathway. Oxid Med Cell Longev. 2020;2020:5390482.
15. Feng F, Cheng P, Zhang H, Li N, Qi Y, Wang H, et al. The protective role of Tanshinone IIA in Silicosis Rat Model via TGF-beta1/Smad signaling suppression, NOX4 inhibition and Nrf2/ARE signaling activation. Drug Des Devel Ther. 2019;13:4275–90.
16. Tong Y, Xu W, Han H, Chen Y, Yang J, Qiao H, et al. Tanshinone IIA increases recruitment of bone marrow mesenchymal stem cells to infarct region via up-regulating stromal cell-derived factor-1/CXC chemokine receptor 4 axis in a myocardial ischemia model. Phytomedicine. 2011;18:443–50.
17. Qian K, Xu H, Dai T, Shi K. Effects of Tanshinone IIA on osteogenic differentiation of mouse bone marrow mesenchymal stem cells. Naunyn Schmiedebergs Arch Pharmacol. 2015;388:1201–9.
18. Shu B, Zhao YJ, Zhao ST, Pan HB, Xie R, Yi D et al. Inhibition of Axin1 in osteoblast precursor cells leads to defects in postnatal bone growth through suppressing osteoclast formation. Bone Res. 2020;8.
19. Jiang F, Tang ZM, Zhang YH, Ju YH, Gao HQ, Sun N, et al. Enhanced proliferation and differentiation of retinal progenitor cells through a self-healing injectable hydrogel. Biomaterials Sci. 2019;7:2335–47.
20. Kleele T, Rey T, Winter J, Zaganelli S, Mahecic D, Perreten Lambert H, et al. Distinct fission signatures predict mitochondrial degradation or biogenesis. Nature. 2021;593:435–9.
21. Pfeilschifter J, Koditz R, Pfohl M, Schatz H. Changes in proinflammatory cytokine activity after menopause. Endocr Rev. 2002;23:90–119.
22. Saul D, Khosla S. Fracture Healing in the setting of Endocrine diseases, Aging, and Cellular Senescence. Endocr Rev. 2022.
23. Naismith E, Pangrazzi L. The impact of oxidative stress, inflammation, and senescence on the maintenance of immunological memory in the bone marrow in old age. Biosci Rep. 2019;39.
24. Mittal M, Siddiqui MR, Tran K, Reddy SP, Malik AB. Reactive oxygen species in inflammation and tissue injury. Antioxid Redox Signal. 2014;20:1126–67.
25. Almeida M, Han L, Martin-Millan M, Plotkin LI, Stewart SA, Roberson PK, et al. Skeletal involution by age-associated oxidative stress and its acceleration by loss of sex steroids. J Biol Chem. 2007;282:27285–97.
26. Hussain T, Tan B, Yin Y, Blachier F, Tossou MC, Rahu N. Oxidative stress and inflammation: what polyphenols can do for us? Oxid Med Cell Longev. 2016;2016:7432797.
27. Leyane TS, Jere SW, Houreld NN. Oxidative stress in Ageing and Chronic degenerative pathologies: molecular mechanisms involved in counteracting oxidative stress and chronic inflammation. Int J Mol Sci. 2022;23.
28. Ferrucci L, Fabbri E. Inflammageing: chronic inflammation in ageing, cardiovascular disease, and frailty. Nat Rev Cardiol. 2018;15:505–22.
29. Ginaldi L, Di Benedetto MC, De Martinis M. Osteoporosis, inflammation and ageing. Immun Ageing. 2005;2:14.
30. Park D, Spencer JA, Koh BI, Kobayashi T, Fujisaki J, Clemens TL, et al. Endogenous bone marrow MSCs are dynamic, fate-restricted participants in bone maintenance and regeneration. Cell Stem Cell. 2012;10:259–72.
31. Chen C, Yan S, Qiu S, Geng Z, Wang Z. HIF/Ca(2+)/NO/ROS is critical in roxadustat treating bone fracture by stimulating the proliferation and migration of BMSCs. Life Sci. 2021;264:118684.
32. Chen M, Sun Y, Hou Y, Luo Z, Li M, Wei Y, et al. Constructions of ROS-responsive titanium-hydroxyapatite implant for mesenchymal stem cell recruitment in peri-implant space and bone formation in osteoporosis microenvironment. Bioact Mater. 2022;18:56–71.
33. Mimeault M, Batra SK. Recent insights into the molecular mechanisms involved in aging and the malignant transformation of adult stem/progenitor cells and their therapeutic implications. Ageing Res Rev. 2009;8:94–112.
34. Ito K, Suda T. Metabolic requirements for the maintenance of self-renewing stem cells. Nat Rev Mol Cell Biol. 2014;15:243–56.
35. Sheppard AJ, Barfield AM, Barton S, Dong Y. Understanding reactive oxygen species in bone regeneration: a glance at potential therapeutics and Bioengineering Applications. Front Bioeng Biotechnol. 2022;10:836764.
36. Ye G, Xie Z, Zeng H, Wang P, Li J, Zheng G, et al. Oxidative stress-mediated mitochondrial dysfunction facilitates mesenchymal stem cell senescence in ankylosing spondylitis. Cell Death Dis. 2020;11:775.
37. Denu RA, Hematti P. Effects of oxidative stress on Mesenchymal Stem Cell Biology. Oxid Med Cell Longev. 2016;2016:2989076.
38. Benameur L, Charif N, Li Y, Stoltz JF, de Isla N. Toward an understanding of mechanism of aging-induced oxidative stress in human mesenchymal stem cells. Biomed Mater Eng. 2015;25:41–6.
39. Panwar P, Xue L, Soe K, Srivastava K, Law S, Delaisse JM, et al. An Ectosteric Inhibitor of Cathepsin K inhibits bone resorption in Ovariectomized Mice. J Bone Min Res. 2017;32:2415–30.
40. Yang Y, Su Y, Wang D, Chen Y, Wu T, Li G, et al. Tanshinol attenuates the deleterious effects of oxidative stress on osteoblastic differentiation via Wnt/FoxO3a signaling. Oxid Med Cell Longev. 2013;2013:351895.
41. Cheng L, Zhou S, Zhao Y, Sun Y, Xu Z, Yuan B, et al. Tanshinone IIA attenuates osteoclastogenesis in ovariectomized mice by inactivating NF-kB and Akt signaling pathways. Am J Transl Res. 2018;10:1457–68.
42. Wang L, Cheng L, Zhang B, Wang N, Wang F. Tanshinone prevents alveolar bone loss in ovariectomized osteoporosis rats by up-regulating phosphoglycerate dehydrogenase. Toxicol Appl Pharmacol. 2019;376:9–16.
43. Zhang J, Cai Z, Yang M, Tong L, Zhang Y. Inhibition of tanshinone IIA on renin activity protected against osteoporosis in diabetic mice. Pharm Biol. 2020;58:219–24.
44. Cui L, Wu T, Liu YY, Deng YF, Ai CM, Chen HQ. Tanshinone prevents cancellous bone loss induced by ovariectomy in rats. Acta Pharmacol Sin. 2004;25:678–84.
45. Li J, He C, Tong W, Zou Y, Li D, Zhang C, et al. Tanshinone IIA blocks dexamethasone-induced apoptosis in osteoblasts through inhibiting Nox4-derived ROS production. Int J Clin Exp Pathol. 2015;8:13695–706.
46. Zhu S, Wei W, Liu Z, Yang Y, Jia H. TanshinoneIIA attenuates the deleterious effects of oxidative stress in osteoporosis through the NFkappaB signaling pathway. Mol Med Rep. 2018;17:6969–76.
47. Keleku-Lukwete N, Suzuki M, Yamamoto M. An overview of the advantages of KEAP1-NRF2 system activation during Inflammatory Disease Treatment. Antioxid Redox Signal. 2018;29:1746–55.
48. Li S, Shi M, Wang Y, Xiao Y, Cai D, Xiao F. Keap1-Nrf2 pathway up-regulation via hydrogen sulfide mitigates polystyrene microplastics induced-hepatotoxic effects. J Hazard Mater. 2021;402:123933.
49. Zhang Y, Jiang P, Ye M, Kim SH, Jiang C, Lu J. Tanshinones: sources, pharmacokinetics and anti-cancer activities. Int J Mol Sci. 2012;13:13621–66.
50. Tong X, Yang F. Recent progress in developing Injectable matrices for enhancing cell delivery and tissue regeneration. Adv Healthc Mater. 2018;7:e1701065.
51. Nelson VJ, Dinnunhan MFK, Turner PR, Faed JM, Cabral JD. A chitosan/dextran-based hydrogel as a delivery vehicle of human bone-marrow derived mesenchymal stem cells. Biomed Mater. 2017;12:035012.
52. Ding X, Li X, Li C, Qi M, Zhang Z, Sun X, et al. Chitosan/Dextran Hydrogel constructs containing strontium-doped hydroxyapatite with enhanced osteogenic potential in rat cranium. ACS Biomater Sci Eng. 2019;5:4574–86.
53. Balakrishnan B, Soman D, Payanam U, Laurent A, Labarre D, Jayakrishnan A. A novel injectable tissue adhesive based on oxidized dextran and chitosan. Acta Biomater. 2017;53:343–54.

54. Zhang W, Shi Y, Li H, Yu M, Zhao J, Chen H, et al. In situ injectable nano-complexed hydrogel based on chitosan/dextran for combining tumor therapy via hypoxia alleviation and TAMs polarity regulation. Carbohydr Polym. 2022;288:119418.
55. Gibbs DM, Black CR, Dawson JI, Oreffo RO. A review of hydrogel use in fracture healing and bone regeneration. J Tissue Eng Regen Med. 2016;10:187–98.

Publisher's Note